Hindawi
Shock and Vibration
Volume 2023, Article ID 6381319, 15 pages
https://doi.org/10.1155/2023/6381319

Research Article

Modeling and Investigation of the Velocity-Dependent Cutting Process with PDC Cutters Using the Discrete Element Method

Zhiyi Fu,[1] **Georg-Peter Ostermeyer**,[1] **Armin Kueck**,[2] **Frank Schiefer**,[1] **Hanno Reckmann**,[3] **Xu Huang**,[2] **and John Bomidi**[2]

[1]*Technische Universität Braunschweig, Institute of Dynamics and Vibrations, Schleinitzstrasse 20, 38106 Braunschweig, Lower Saxony, Germany*
[2]*Baker Hughes, 9110 Grogans Mill Rd, The Woodlands, 77380 Texas, USA*
[3]*Baker Hughes, Baker-Hughes-Str. 1, 29221 Celle, Lower Saxony, Germany*

Correspondence should be addressed to Georg-Peter Ostermeyer; gp.ostermeyer@tu-braunschweig.de

Received 13 August 2022; Revised 27 October 2022; Accepted 31 October 2022; Published 20 February 2023

Academic Editor: Reza Taherdangkoo

Polycrystalline diamond compact (PDC) bits with multiple fixed cutters drill through deep formations and are used in oil and gas, geothermal, and mining industry. The bit-rock interaction excites drill string vibrations, which need to be mitigated to improve drilling performance. A velocity-weakening characteristic of the bit torque can cause severe self-excited high-frequency torsional oscillations (HFTO) of the bottom hole assembly (BHA). The dependency on velocity can be attributed to rate-sensitive rock cutting forces at each cutter. The purpose of this paper is to model the rate effect of cutting forces and determine influencing factors in the single-PDC cutting process. In this paper, a modified bonded-particle model (discrete element method, DEM) for rock in deep drilling environments is applied to the pressurized cutting process. Potential modification strategies considering rate indicators at different scales are compared and discussed to reproduce rate dependency in the particle contact model. Two specific models, incorporating cutting-speed-dependent bond strength or grain elastoplasticity, are implemented and verified. The relationship between rate-sensitive cutting forces and the causal rock failure mechanisms is then clarified by interpreting the results from a continuum perspective. Moreover, the influences of axial force and cutter wear state on the rate dependency are investigated. In cutting simulations at a constant depth of cut and various cutting speeds, both models result in rate-dependent cutting forces in good qualitative agreement with rock experiments: Significant hardening is reflected in the axial force component. The modification of contact models combined with a macroscopic rate indicator (i.e. cutting speed) has proven to be a feasible and effective way to reproduce the rate effects in the cutting simulations. In subsequent simulations with constant axial force, the steady-state tangential force decreases as the cutting speed increases, matching the reduction of torque on the bit with increasing RPM. Rate dependency intensifies at higher axial forces or with dull cutters, which agrees with laboratory full-scale bit tests in the literature. This study proposes a practical approach to integrating observed rate effects of downhole rock cutting processes into numerical rock models. The results enhance our understanding of the rock cutting process and have positive implications for the improvement of the cutter design against undesirable rate effects.

1. Introduction

In the deep earth drilling process, polycrystalline diamond compact (PDC) bits with multiple fixed cutters (see also Figure 1(a)) are widely used to drill through rock formations. The bit-rock interaction often causes severe drill-string vibrations that occur in the axial, lateral, and torsional directions. Among these unwanted vibrations, self-excited high-frequency torsional oscillations (HFTO) of the bottom hole assembly (BHA) often dominate the drill-string dynamics, leading to critical premature failures of downhole components [2]. When this vibration type occurs, the BHA vibrates at a single eigenfrequency of the drill string between 50 and 400 Hz [3]. This self-excited phenomenon is primarily caused by a velocity-dependent torque characteristic in the bit-rock interaction while drilling hard and dense

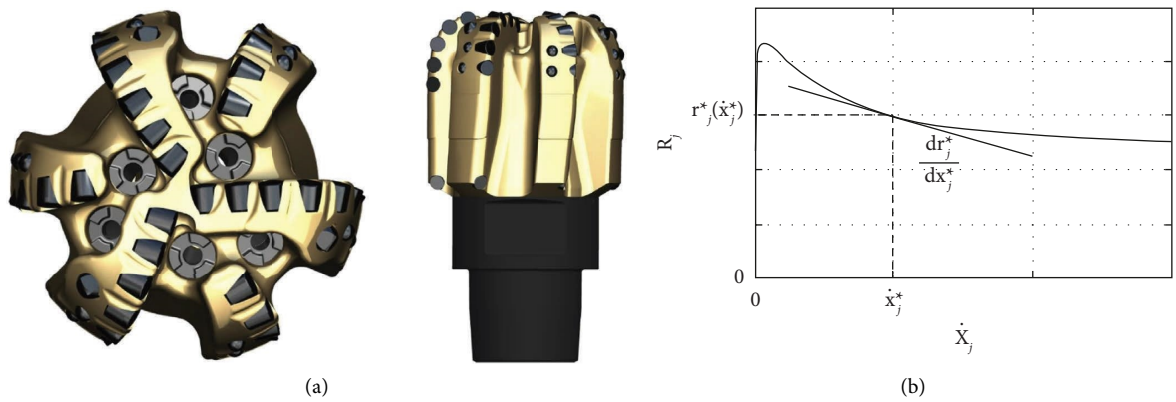

(a) (b)

Figure 1: (a) Example of PDC bits; (b) velocity-dependent torque characteristic [1].

formations [1]. The torque on bit (TOB) decreases as the rotary speed (i.e. RPM) increases, creating a negative slope at an operating point and thus destabilizing the drill string system due to energy inflow, as illustrated in Figure 1(b). Consequently, self-excited torsional vibrations arise if the system damping is not sufficient to dissipate this energy input from the excitation.

To explain the genesis of the falling torque characteristic with increasing RPM, the first argument is focused on whether the falling torque characteristic is primarily associated with rock properties. Richard et al. [4] claimed that the torque characteristic is not an intrinsic property of the bit-rock interface, but an indirect consequence of drill string vibrations (or stick-slip in this context). The authors introduced a state-dependent but cutting-rate-independent bit-rock interaction model into a two-degree-of-freedom drill string model and managed to reproduce stick-slip in their simulations. Accordingly, the observed falling torque characteristic results from the reduction in depth of cut (DOC) due to the decreased intensity of axial vibrations at higher RPM. However, this theory holds true only if the modal frequency interval between the low-frequency torsional mode and the high-frequency axial mode is large enough. This condition is not satisfied for HFTO, where a strong coupling of torsional and axial vibrations with the same high frequency is observed [5]. In this case, a more convincing explanation is that the falling characteristic is rooted in a constitutive rate dependency in the bit-rock interaction.

Since bit-rock interaction can be considered as the combination of all cutter-rock interactions on the bit, the velocity-weakening torque characteristic can be attributed to the rate-dependent rock cutting process at each cutter, i.e, the tangential cutting force decreases with increasing cutting velocity. Theoretically, this rate sensitivity could result from two potential aspects: either the reduction in tangential cutting force is a direct outcome of rock weakening at a higher velocity, or it could indirectly come from a mechanism that lowers the depth of cut (DOC) at a higher velocity because the tangential cutting force decreases with reduced DOC. In the first case, the rate dependency is an uncoupled behavior restricted in the tangential direction, which is independent of the axial dynamics. For the latter case, the reduction of DOC over cutting velocity can be accomplished by the rate hardening of the axial cutting force, implicating a tangential-axial coupling effect. In this situation, the axial force increases with increasing cutting speed, thus creating an additional velocity-dependent lift force on the bit. Then the drill bit is lifted if the weight on the bit (WOB) remains constant, which is an usual case in standard drilling operations. Several laboratory studies on the rock cutting process with a single PDC cutter have supported the latter hypothesis about the axial rate hardening effect, for example in [6, 7].

If the velocity-dependent cutting process with PDC cutters is the root cause of the falling torque characteristic, fundamental strategies for reducing and mitigating the self-excited HFTO can be deduced through modeling the rate hardening effect of cutting forces and investigating the influence factors. Several studies have attempted to model the rate-dependent cutting process using diverse physical explanations. Based on the experimental observation of a shear rate strengthening effect in granular systems in [8], Pelfrene et al. [6] added a logarithmic formulation between the cutting speed and the normal stress on the wear flat into the cutting force model for a PDC cutter. With the same motivation, Matthews et al. [9] also included a velocity-dependent term in their drilling force model, achieving better agreement between simulated and laboratory test data. However, these simplified modifications only give a phenomenological description of the observed rate effect but are not usable to explore the influencing factors.

Another explanation comes from the theory of poroelasticity. The saturated rock formation at the pressurized bottom hole is a porous material. Therefore, the interaction between pore pressure dynamics and rock mechanical properties has an additional impact on the rock cutting process. With this consideration, Kolle [10] and Detournay and Atkinson [11] developed two similar analytical models to describe the dynamic confining pressure due to different pore pressure reductions on the shear dilatant plane at different cutting speeds. Thereafter, Amri et al. [12] and Chen et al. [13] independently extended the poroelastic modeling of the PDC cutting process by introducing solid-

fluid coupling to obtain stress and pore pressure fields in the rock. However, the rate effect caused by pore pressure diffusion only applies to rocks with high permeability, which cannot explain the self-excited HFTO in hard and low-permeable formations [5]. Moreover, the application of these analytical models is limited to simple boundary conditions that are not able to describe the realistic cutter-rock interface with various geometric configurations.

Instead of analytical approaches, numerical simulations are appropriate substitutions for studying the cutter-rock interaction during the rock cutting process. Compared with other numerical modeling methods, the discrete element method (DEM) is a favorable candidate due to its advantages in effectively accommodating the large deformations and fractures involved in rock cutting processes. Therefore, several studies have used DEM to simulate the rock cutting process with PDC cutters and to investigate various influencing factors [14–17]. Through these DEM investigations, the understanding of cutter-rock interaction has been enhanced. However, to the authors' knowledge, modeling of the above-mentioned rate dependency has rarely been covered in DEM cutting simulations. Helmons et al. [18] incorporated pore pressure modeling in DEM using smoothed particle techniques. However, diverse dynamic properties of rock materials can also accomplish the rate effects in the cutting process rather than being restricted to this physical mechanism that is negligible in low-permeability rocks. As reviewed by Zhang and Zhao [19], rate-dependent rock properties were commonly observed in various dynamic tests. Besides fluid diffusion, other aspects of rock properties should be explored in DEM modeling regarding rate dependencies, such as inertia effects, viscous behavior or dynamic fragmentation [19].

This paper aims at modeling and investigating rate dependency in the PDC cutting process based on DEM simulations developed in our previous studies [20, 21]. In the first part, experimental cutting tests with a single PDC cutter are conducted and evaluated to obtain the characteristics of the rate dependency of cutting forces. Then different modeling strategies of DEM for reproducing the observed rate dependency are discussed, and two potential contact models incorporating cutting-speed-dependent parameters are implemented. Interpreting the cutting simulation results from a continuum perspective explicitly reveals the relationship between rate-dependent cutting forces and the causal rock failure mechanisms. Finally, the influences of typical operating and geometrical parameters on the rate dependency are investigated and compared with laboratory tests reported in the literature.

2. Experimental Cutting Tests

2.1. Single Cutter Test Rig. To characterize the rate dependency in the rock cutting process, single cutter tests under hydrostatic confining pressure were conducted on a test rig [22]. The test rig mainly consists of a pressure vessel and a cutter shaft. A rock sample plate is placed in the vessel that is pressurized with fluid to simulate the confining bottom-hole pressure. The cutter shaft is equipped with a load cell and its movement is controlled by a hydraulic servo system.

The schematic of the cutting test inside the pressure vessel is shown in Figure 2. In these tests, the single cutter mounted on the load cell moves vertically down to penetrate the rock sample at a prescribed velocity. Meanwhile, the rock sample rotates at a constant RPM so that a stable DOC is reached after the first revolution. The vertical displacement of the cutter, the rotational speed, and the cutting forces in three directions (axial, tangential, and radial) are measured and recorded. The cutting area can be geometrically calculated from the displacement signal.

2.2. Characterization of Rate Dependency. In this study, all tests are performed with a 16 mm diameter cutter with a 0.016 inch chamfer at a 20° back rake angle. Danby Marble is chosen as the rock specimen under 3000 psi confining pressure. To study the rate sensitivity of cutting forces, the tests are conducted at various rotational speeds and the same DOC. The raw signals of the cutting forces are divided into a smoothed and a noise part first using a low-pass filter. According to statistical and FFT analyses, the noise signal follows a normal distribution and demonstrates no obvious peak values in its frequency spectrum. Consequently, the noise can be neglected in further analysis.

The smoothed cutting forces at different cutting speeds are shown in Figure 3. Since the cutting forces in the normal and tangential direction at the single cutter correspond to the weight on bit (WOB) and torque on bit (TOB), respectively, the test data evaluation will focus on these two directions. The results indicate that cutting forces increase with the number of revolutions because the area of cut (AOC) keeps increasing during the cutting process with a single cutter and more energy for rock fragmentation is consumed. In addition, a distinct hardening effect with increasing RPM is found in the axial component, whereas the tangential force remains roughly independent on the cutting speed. This observed rate effect is consistent with the results on another rock type (Anstrude limestone) reported by Pelfrene et al. [6].

The rise of the cutting forces in single cutter tests with unsteady AOC is not encountered while drilling with a full bit because the cutting area in front of an individual cutter overlaps with the grooves left by the previous cutter trajectories [24]. To eliminate the influence of increasing AOC, linear regression is performed based on the correlation analysis that shows that cutting forces strongly correlate with AOC among all test data. The data from the first revolution are ignored because the DOC does not reach a constant state yet. Following the definitions in [25], the drilling strength (DS) and the specific energy (SE) are obtained for each test, as shown in Figure 4. These two characteristic values represent the axial and tangential force components normalized to the AOC, respectively. The cutter's aggressiveness, defined as the ratio of tangential and axial force, is given as well.

As can be seen, an obvious RPM-dependent hardening effect of DS systematically appears, while SE is nearly independent of RPM. In other words, a higher axial force is required to maintain the same DOC at a higher tangential cutting speed, while the tangential force does not change noticeably. This results in a falling characteristic of

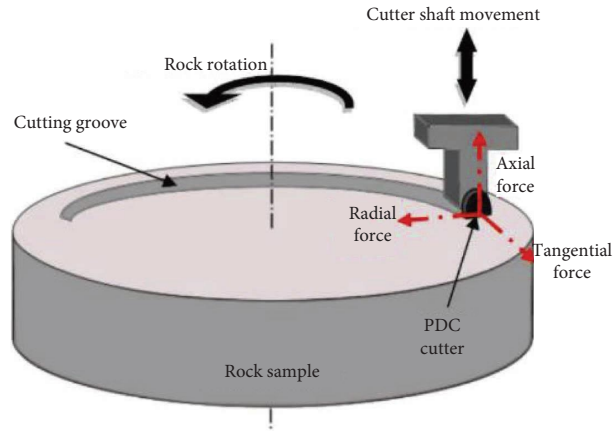

Figure 2: Schematic diagram of the single cutter test. [23].

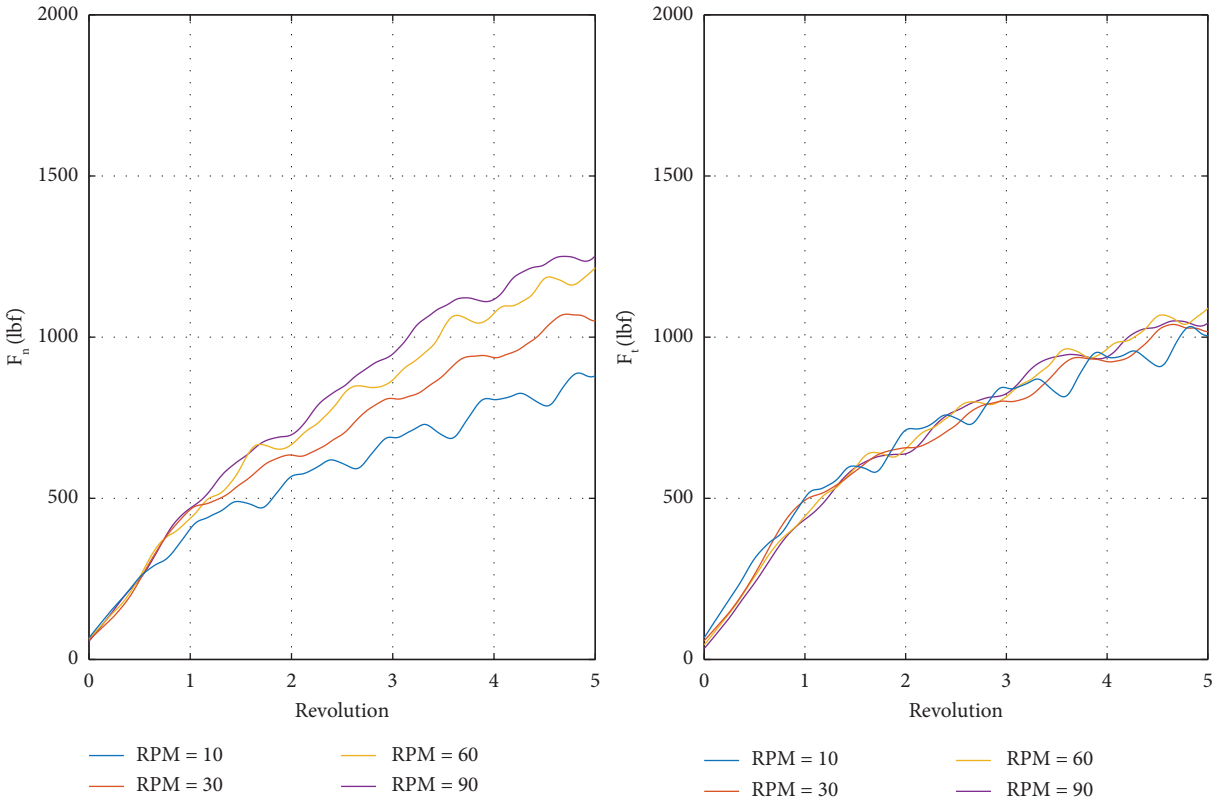

Figure 3: Smoothed axial (F_n) and tangential (F_t) cutting forces with various cutting speeds.

aggressiveness over the rotational speed. As discussed, this velocity-dependent characteristic could be the cause of self-excited drill string oscillations. To enhance the understanding of self-excitation, this observed RPM effect will be incorporated into the DEM modeling.

3. Modeling and Simulation

3.1. DEM Simulation of the Rock Cutting Process. As a starting point for further modifications concerning the rate dependency, the DEM base model and the rock cutting simulation are introduced in this section first. To model a granular material such as rock, the DEM explicitly considers individual particles and their interactions. The motion of each particle is governed by the following equation:

$$m_i \ddot{\mathbf{u}}_i = \mathbf{F}_i + \sum_j \mathbf{F}_{ji},$$
$$\Theta_i \dot{\boldsymbol{\omega}}_i = \mathbf{M}_i + \sum_j \mathbf{M}_{ji}, \quad (1)$$

where $\ddot{\mathbf{u}}_i$ is the translational acceleration vector and $\dot{\omega}_i$ is the angular acceleration vector for particle i, m_i is the mass, Θ_i is the moment of inertia, $\mathbf{F}_i$ and $\mathbf{M}_i$ are external forces and

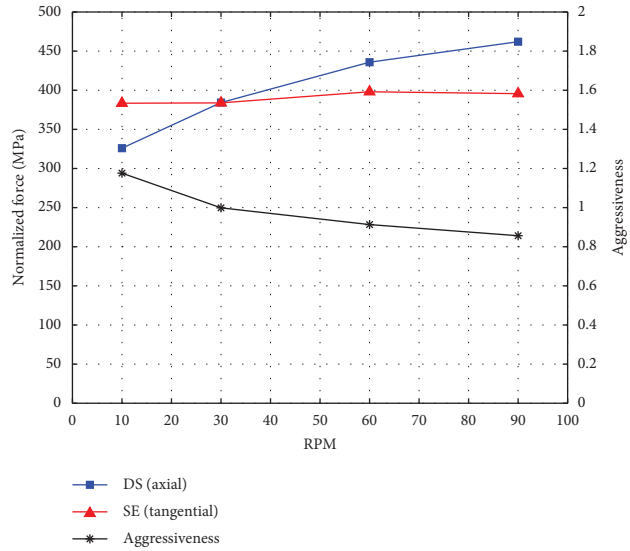

Figure 4: Evaluated drilling strength (DS), specific energy (SE), and cutter aggressiveness.

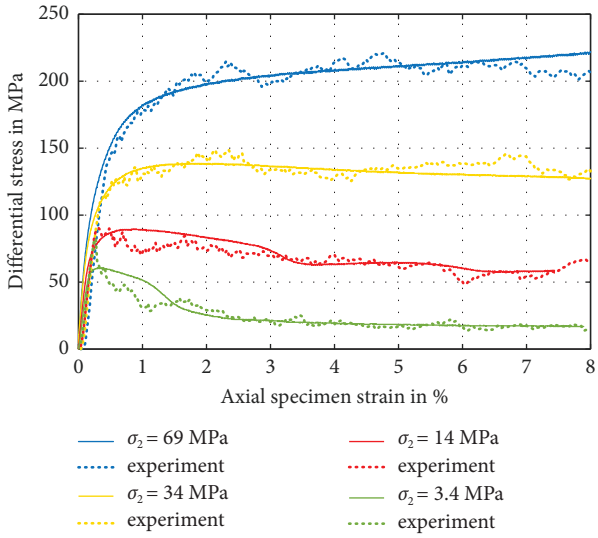

Figure 5: Simulated and measured results of triaxial compression tests on Danby marble.

torques, and $\mathbf{F}_{ji}$ and $\mathbf{M}_{ji}$ are the contact forces and torques due to interactions with other particles or boundaries.

The particulate interactions determine the mechanical behavior of the granular system. The corresponding contact forces are calculated by a constitutive contact model that describes the force-displacement law at each contact. For rock materials, a bonded-particle model proposed by Potyondy and Cundall [26] is often used, which decomposes the contact forces into different directions and portions as denoted by the following equations:

$$F_{\mathrm{n}} = F_{\mathrm{n}}^{\mathrm{p}} + F_{\mathrm{n}}^{\mathrm{b}} + F_{\mathrm{n}}^{\mathrm{d}},\ F_{\mathrm{t}} = F_{\mathrm{t}}^{\mathrm{p}} + F_{\mathrm{t}}^{\mathrm{b}} + F_{\mathrm{t}}^{\mathrm{d}},\ M = M^{\mathrm{p}} + M^{\mathrm{b}}, \quad (2)$$

where n stands for normal direction, t for tangential direction, p for particle portion, b for bond portion, and d for damping portion.

This nomenclature also suggests the additional rolling resistance torque M^{p} due to the particle irregularity, as proposed by Tergeist et al. [27]. A previous study has shown that this modification contributes to a better agreement with triaxial compression test data.

To calibrate the parameters of the DEM model for the Danby Marble used in this study, triaxial compression simulations under several confining pressures are conducted. The simulated stress-strain curves are compared with the experimental data on Danby Marble, as shown in Figure 5. A good agreement with the test data is achieved over a large range of strains and confining pressures by selecting proper model parameters. Several relevant calibrated parameters are listed in Table 1. More details about the model parameters and calibrations can be found in [20, 21].

To investigate the rock-cutter interaction, the calibrated DEM model is applied to the implemented two-dimensional cutting simulation, as illustrated in Figure 6. The rock specimen, consisting of bonded particles is constrained by rigid frictional walls on the right and bottom sides. Along the left and upper surfaces, a hydrostatic pressure boundary is realized through a pressure application algorithm developed by Tergeist [20]. The compressive uniform load that simulates the fluid confinement is applied to the identified particle surface chain, except for the dry contact between the cutting chip and the cutter (red particles in Figure 6). The profile of the PDC cutter is represented by mesh segments with a constant coefficient of friction. The cutter movement is separately defined in two orthogonal directions. A constant horizontal velocity is applied in the tangential direction, while either a constant DOC or a constant vertical force is applied in the axial direction, depending on different operating conditions. In the former case, the position and velocity of the cutter are completely prescribed and are not affected by its interaction with particles. For the latter case, a PID-controlled servo wall for the cutter is adopted to achieve force equilibrium in the axial direction.

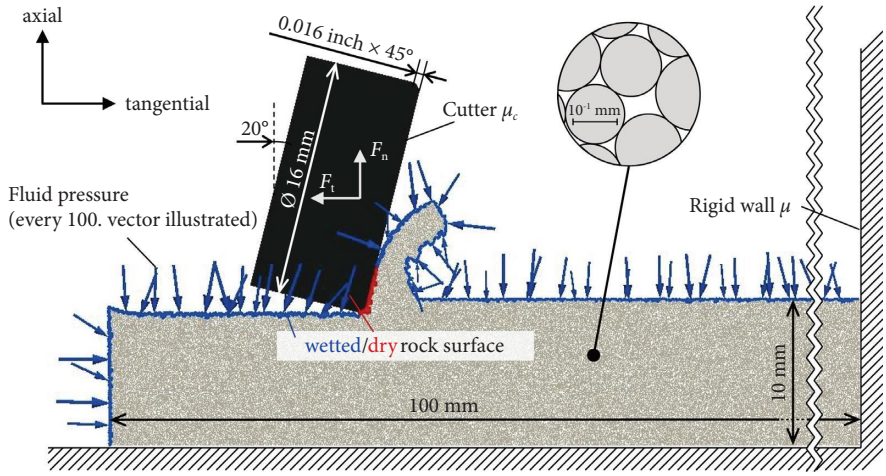

Figure 6: Boundary conditions in the DEM cutting simulation.

Table 1: Calibrated microparameters of the DEM model.

Name	Symbol (unit)	Value
Particle radius	R (μm)	300 ± 75
Density	ρ (kg/m^3)	2630
Elastic modulus	E (GPa)	62
Ratio of normal to shear stiffness	κ (−)	2.5
Coefficient of friction between particles	μ (−)	0.7
Normal bond strength	σ_m (MPa)	125 ± 25
Shear bond strength	τ_m (MPa)	125 ± 25
Initial free-rolling angle	α_f (°)	0.25 ± 0.05
Rolling resistance moment in the plastic phase	$\widehat{M}$ (Nm)	33

3.2. Modification Strategies. To reproduce the experimentally observed rate dependency, the contact model of the DEM is further modified. In the single cutter tests, the rate dependency is characterized by the cutting speed (i.e. RPM), whereas for the DEM contact model, the rate indicator is only reflected in the relative velocities between particles. These two velocity measures are on different geometric scales. Choosing which velocity measure to incorporate the rate dependency is, thus, a primary option for different modification strategies.

The other attribute to be selected is the model complexity. The least complex modification is the introduction of characteristic curves instead of constants for the existing parameters in the DEM contact model. In comparison, adding more rheological elements to modify the force-displacement law is a more complex extension, but with more degrees of freedom. The most complex modification can be accomplished by considering and modeling additional physical mechanisms such as fluid-solid coupling, hydraulic fracturing, and heat transfer. This is usually associated with very specific application scenarios and is beyond the scope of this study.

Through combinations of different choices for these two attributes, various modeling strategies regarding the rate dependency are generated, as schematized in Figure 7. The feasibility and specific implementation of each strategy are further discussed.

3.3. Model Modification with Microscopic Rate Parameters. Considering the complexity and intuitiveness of the implementation, the most convenient approach to extending the contact model is to introduce parameters or rheological elements related to the contact velocity between particles, namely Strategies A and B marked in Figure 7. However, the relative velocity field during the cutting process has a non-uniform spatial distribution that depends on the particle flow driven by the cutter movement and geometry [15]. Therefore, the relationship between the local contact velocities and the macroscopic cutting speed must first be clarified to check the feasibility of modifications using the microscopic rate parameter. This request is compatible with the advantage of DEM simulations in that the positions and velocities of the discrete particles and the contact forces of the particle pairs at each numerical step are available for an in-depth feasibility analysis.

For this purpose, the normal contact forces and the relative velocities at different cutting speeds are compared, as shown in Figure 8. The results are time-averaged over the whole cutting distance using the previously developed averaging approach [21] to achieve a better statistical representation. As can be seen, the higher normal forces concentrate primarily under the chamfer surface. Our previous study [21] also showed a consistent phenomenon in the volumetric stress by which a crush zone was identified. Correspondingly, this concentration of stresses or contact

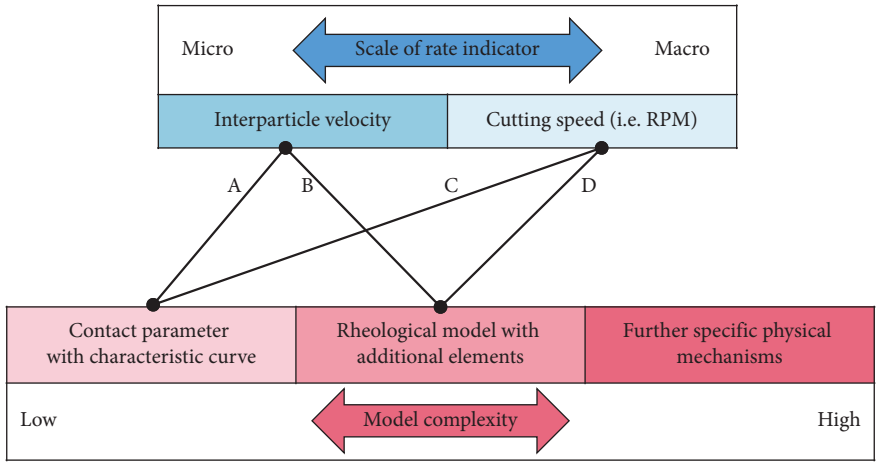

Figure 7: Modification strategies with respect to the rate dependency.

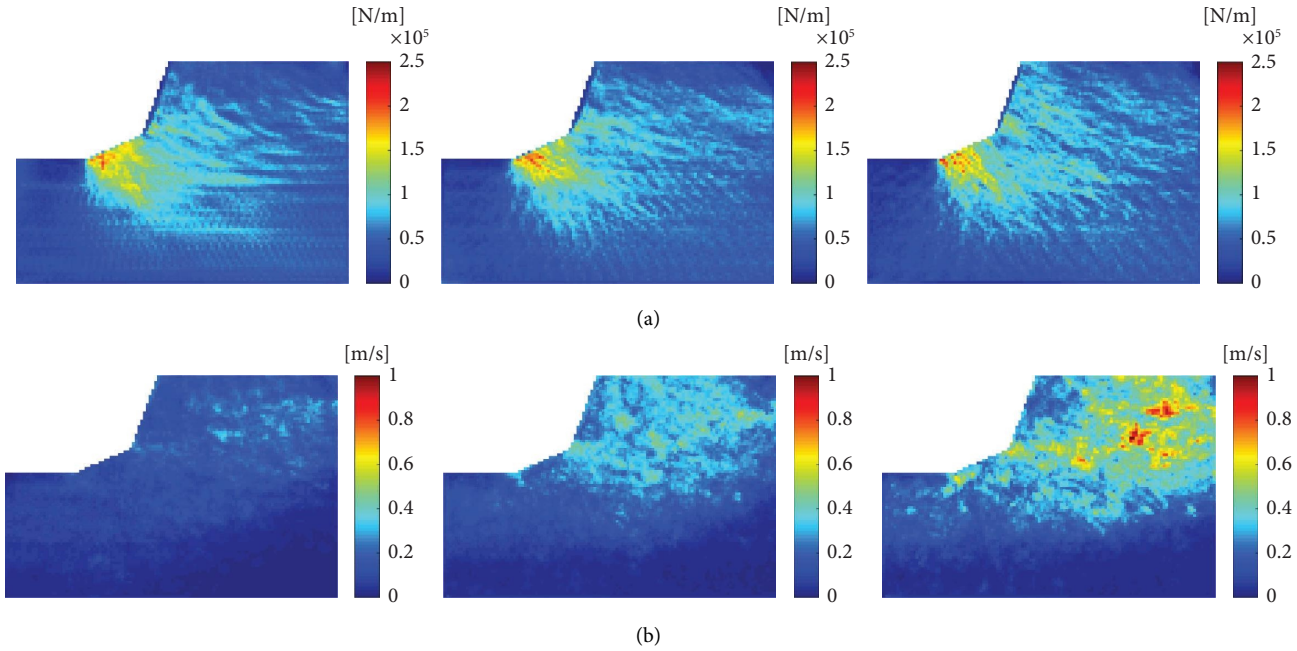

Figure 8: Averaged normal contact force (a) and averaged relative velocity (b) with various cutting speeds (30, 60, and 90 RPM from left to right).

forces has a decisive influence on the axial cutting force. Therefore, modifications for the observed axial hardening effect should also take effect in this region. In contrast, the change of the relative velocity field at different cutting speeds appears in other regions where the shear zone is formed in front of the cutter face. This contradiction implies that modifications based on interparticle velocities are not sufficient to reproduce rate-dependent compression behavior. Instead, the macroscopic cutting speed should be involved as the rate indicator to modify the contact model.

3.4. Model Modification with Macroscopic Rate Parameters

3.4.1. Rate-Dependent Normal Bond Strength. For modifications with macroscopic rate parameters, the simplest way is to make the existing parameters of the bonded-particle model dependent on the cutting speed (Strategy C marked in Figure 7). For this purpose, a thorough sensitivity analysis of the contact parameters is performed to investigate their influences on the cutting force responses. The normal bond strength is then found to be the only

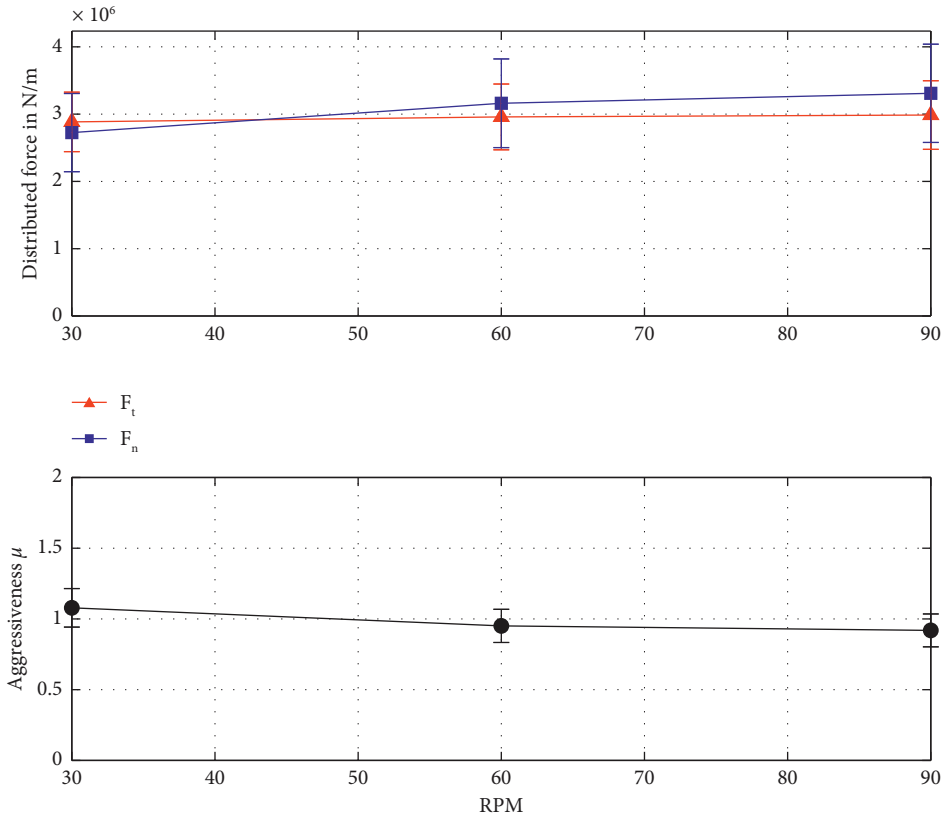

Figure 9: Averaged forces and aggressiveness at various cutting speeds using the model with rate-dependent normal bond strength.

parameter that leads to a dominant increase in the axial cutting force when it is increased. This result implies an appropriate modification by incorporating a normal bond strength related to the cutting speed. To verify the feasibility of this modification, DEM cutting simulations are conducted at a constant DOC and three different cutting speeds (i.e. RPM), while the normal bond strength is varied in each simulation run. To keep it simple, the relationship between the normal bond strength and the cutting speed is set to be linear. The other calibrated model parameters stay the same.

Figure 9 shows the simulated time-averaged force responses and the resultant cutter aggressiveness at various cutting speeds ranging from 30 rev/min to 90 rev/min. Note that a virtual depth of 1 m is assumed in the third dimension for a physical interpretation. The force is thus denoted as a quantity per unit length. The shape of the cutting groove is assumed to have a negligible effect on the cutting forces. It can be seen that the axial cutting force demonstrates a more pronounced tendency to increase with increasing cutting speed, which generates a falling characteristic in aggressiveness over RPM. This consistency with the rate dependency observed in single cutter tests validates the good functionality and reproducibility of applying this modification strategy. Further parameterization reveals that the rate dependency provided by the normal bond strength with cutting speed dependency is limited because the bond strength only takes effect if the bond is not broken. However, the neighboring bonds of the particles near the cutter edge are usually all broken in the cutting simulations. This phenomenon was also observed in the PDC cutting experiments, where the intact rock next to the single cutter surface was pulverized into loose grains [28].

3.4.2. Rate-Dependent Grain Elastoplasticity. To extend the rate dependency, more aspects should be considered by introducing additional degrees of freedom into the contact model. Preceding DEM cutting simulations [14] have shown that the energy consumed by the plastic deformation of the crushed rock under pressure is much higher than the energy dissipated on breaking the bonds between particles. In the base model of the bonded-particle method, rock plasticity is represented through bond breakage, the interparticle frictional contact and rolling resistance. The particle size is predetermined by a uniform distribution and is thereafter assumed to be unchangeable because only elastic and viscous elements are applied in the normal contact direction. In contrast, rock grain crushing was observed by Richard et al. [29] in rock cutting tests. This plasticity of crushed grains is also supported by the quantitative investigation on the cuttings size [30]; the distribution of the cuttings size has a broad range from chunklike particulates to fine powder. Mendoza et al. [31] incorporated the particle-crushing effects into DEM by explicitly implementing crushable particles. However, simulating the event of a particle splitting

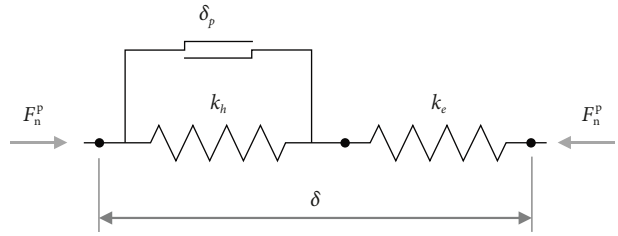

Figure 10: Schematic diagram of the elastoplastic normal contact model for particle portion.

into smaller particles is an unstable and computationally intensive task [32].

As a substitute, an abstract formulation for elastoplasticity is deployed in the normal contact model of the grain portion. An additional module consisting of a slider element for plasticity and a second spring for hardening is connected in series with the original spring for elasticity, as illustrated in Figure 10. The slider controls the onset of the plastic stage through a threshold value δ_p for the overlap. This elastoplastic contact model is mathematically expressed by the following equations:

$$F_n^p = \begin{cases} k_e\delta, \text{if } \delta_{\max} \le \delta_p, \\ k_e\delta_p + k_h\left(\delta - \delta_p\right), \text{if } k_e\left(\delta - \delta_0\right) \ge k_e\delta_p + k_h\left(\delta - \delta_p\right) \text{ and } \delta_{\max} > \delta_p, \\ k_e\left(\delta - \delta_0\right), \text{if } 0 \le k_e\left(\delta - \delta_0\right) < k_e\delta_p + k_h\left(\delta - \delta_p\right) \text{ and } \delta_{\max} > \delta_p, \\ 0, \text{if } k_e\left(\delta - \delta_0\right) < 0 \text{ and if } \delta_{\max} > \delta_p. \end{cases} \tag{3}$$

where k_e is the elastic stiffness, k_h is the hardening stiffness, δ is the overlap, $\delta_{\max}$ is the maximum overlap, and δ_0 is the residual overlap at which the force decreases to zero during the unloading phase.

Note that the maximum overlap $\delta_{\max}$ is a history variable that is continuously updated since the beginning of contact. The residual overlap δ_0 is calculated by the following equation:

$$\delta_0 = \left(1 - \frac{k_h}{k_e}\right)\left(\delta_{\max} - \delta_p\right). \tag{4}$$

The corresponding piecewise force-displacement relationship is shown in Figure 11. The energy loss due to the unrecoverable plastic deformation is dissipated by the hysteresis damping that occurs in the contact cycles throughout the loading and unloading phases. This energy dissipation is decoupled from the local contact velocity and can be better controlled to achieve various behaviors of grain elastoplasticity.

This modified normal contact model is then integrated into the existing DEM model. The sensitivities of the cutting force respond to both additional contact parameters (i.e. δ_p and k_h) are then investigated. It is found that the axial cutting force increases faster than the tangential force as the yield threshold δ_p increases, while the hardening stiffness has effects in both directions in equal measure. Therefore, the observed rate effect of axial force can be reasonably reproduced by the yield threshold, depending on the cutting speed (Strategy D in Figure 7). The threshold overlap δ_p is chosen to be 2e−6 m as a reference value and increases linearly with the cutting speed. Other additional parameters for the grain elastoplasticity are selected through systematic parametric sensitivity studies to ensure their effectiveness in the considered range of cutting speed. Accordingly, a more significant increase of axial force with increasing cutting speed is obtained from the cutting simulations, which eventually leads to the velocity-weakening characteristic of the cutter aggressiveness, as shown in Figure 12. This modification with grain elastoplasticity takes effect mainly after bond breakages and thus complements the rock rate dependency in its full degradation during the PDC cutting process.

4. Discussion

4.1. Causal Rock Failure Mechanisms. In contrast to the empirical model [6], the two modifications produce more than merely phenomenological representations of the observed rate dependency in the cutting process. Instead, they connect the macroscopic cutting speed with the microscopic contact parameters (i.e. the normal bond strength and the yield threshold). Therefore, the macroscale rate dependency is generated from interactions of microscale particles during the rock failure process in the cutting simulations. To understand the root cause, the corresponding simulation results are postprocessed from the continuum perspective using the approach in our previous study [21]. The volumetric stresses are derived from the contact forces and the locations of particles and then averaged over the whole cutting distance.

Figure 13 depicts the obtained volumetric stress distributions at two different cutting speeds using the two modifications, respectively. It can be seen that the stress distribution is changed if considering the grain plasticity; the

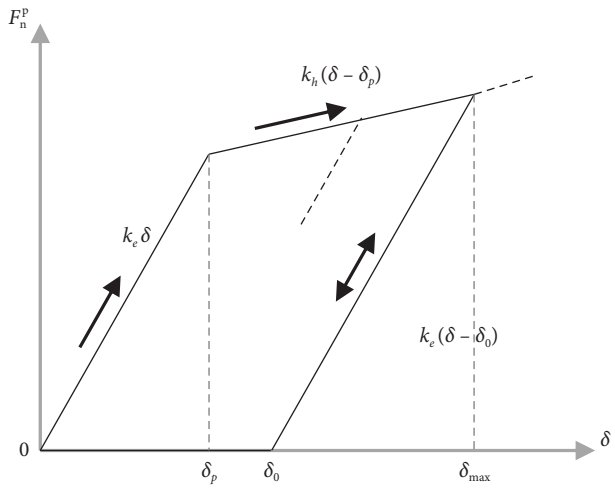

Figure 11: Elastoplastic force-displacement law in the normal direction.

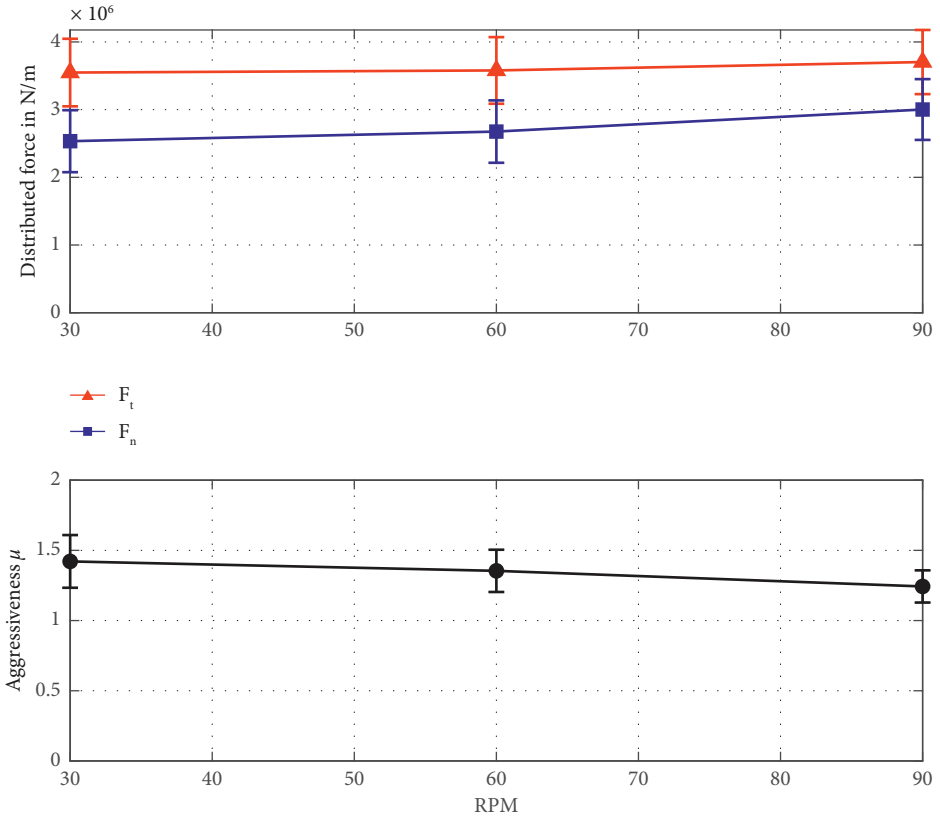

Figure 12: Averaged forces and aggressiveness at various cutting speeds using the model with rate-dependent grain elastoplasticity.

stress concentration in the crush zone below the chamfer is reduced, and more support for the cutter is created by the compressed cuttings in front of the cut face. Nevertheless, the rate dependency simulated by both modified rate-dependent models still results from the increase in stress concentration at higher cutting speeds. This implies a strong correlation between the rate-hardening effect of the axial cutting force and the compression behavior of the crushed rock below the chamfer. In this way, the causal rock failure mechanisms for the simulated rate dependency are revealed.

4.2. Falling Characteristics over RPM. The falling characteristic over RPM is reflected by the cutter aggressiveness in the above simulations with a constant DOC using the two modified models incorporating the rate dependency. In the

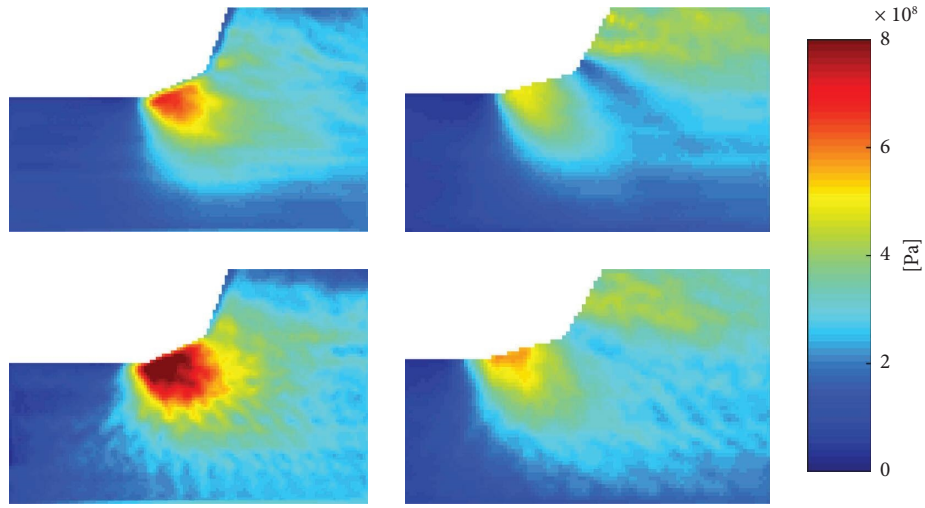

Figure 13: Averaged volumetric stress with 30 RPM (top) and 90 RPM (down) using models with rate-dependent normal bond strength (left) and grain elastoplasticity (right).

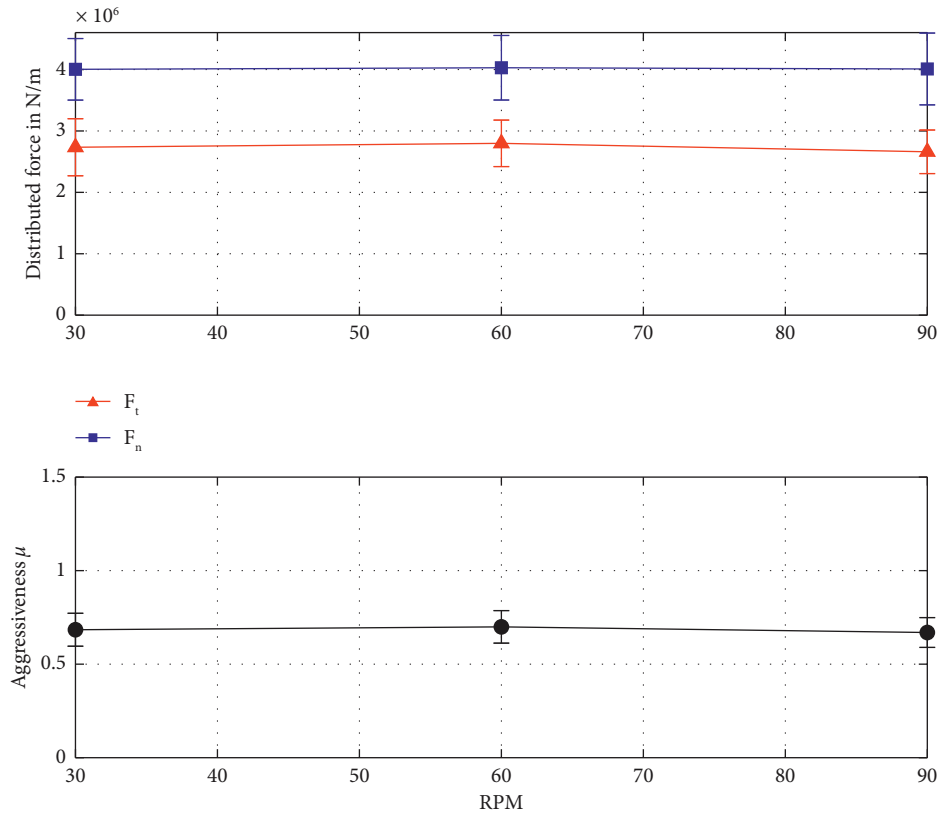

Figure 14: Averaged forces and aggressiveness at various cutting speeds under constant axial force control using the rate-independent model.

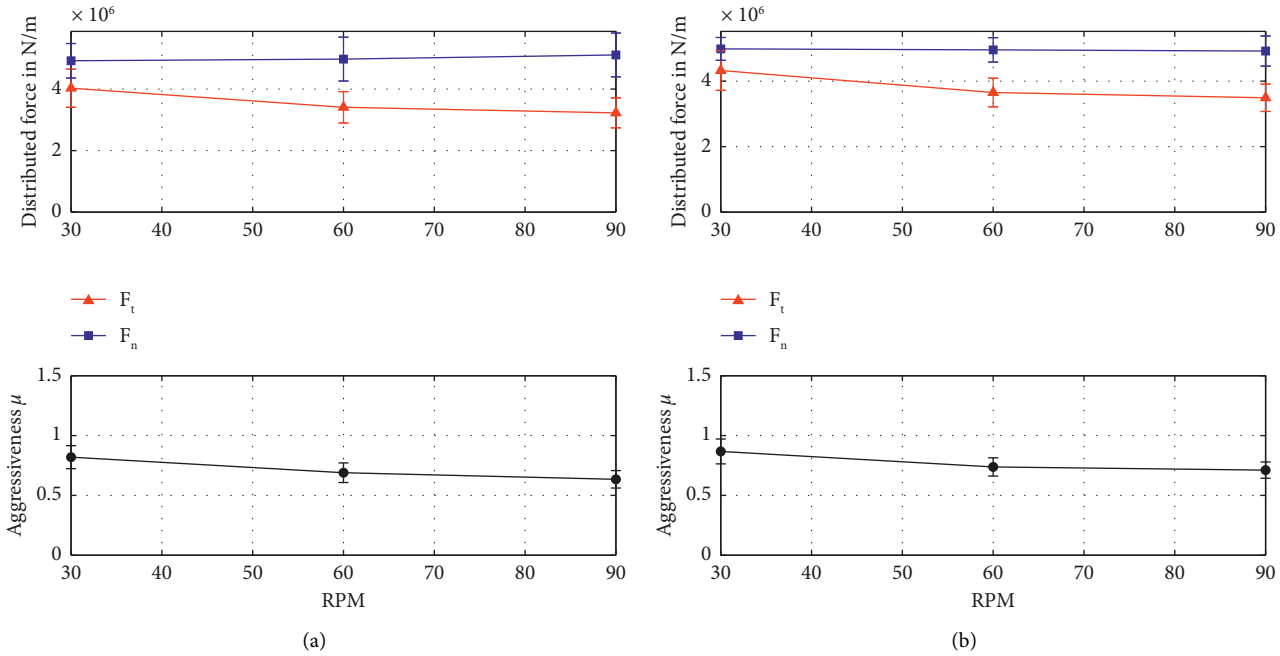

Figure 15: Averaged forces and aggressiveness at various cutting speeds under constant axial force control using models with rate-dependent (a) normal bond strength and (b) grain elastoplasticity.

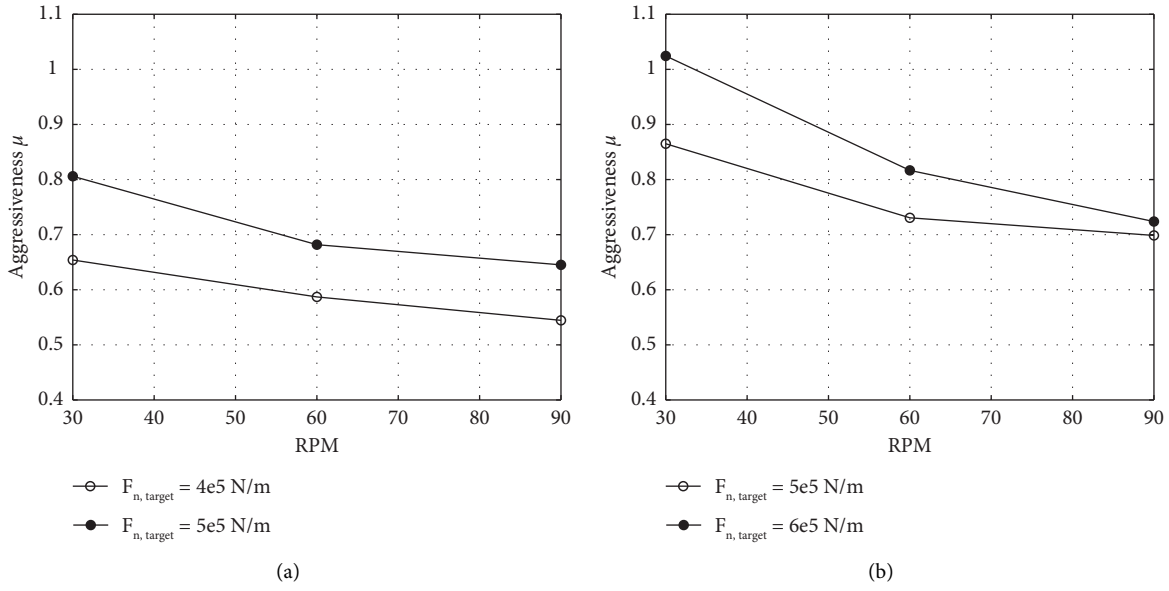

Figure 16: Effect of axial force using the models with cutting speed dependency on (a) normal bond strength and (b) grain elastoplasticity.

drilling process with a full drill bit, the falling characteristic over RPM appears more often in the torque on the bit when WOB is held constant, as observed by some measurements both in the laboratory and in the field [6, 33, 34].

To verify the falling characteristic under similar boundary conditions in the cutting process with a single cutter, DEM simulations with a constant axial force control are conducted at various cutting speeds. A PID controller is used to achieve the target force in the axial direction while the tangential cutting speed is prescribed with a constant value. The steady-state cutting forces in both directions are averaged. With the rate-independent material model, no perceptible change occurs in the tangential direction, as shown in Figure 14.

By contrast, a falling characteristic of the averaged tangential force with respect to the RPM is obtained using both cutting-speed dependent models, as shown in Figure 15. This falling characteristic is caused by the incorporated rate dependency. At higher tangential speeds, the force response in the axial direction becomes larger, pushing

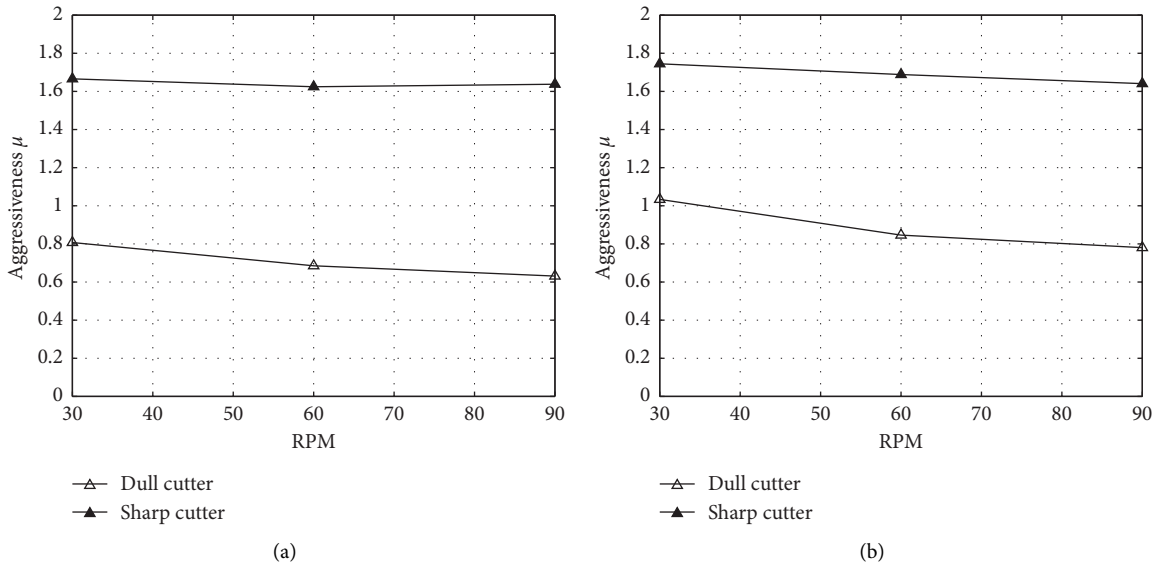

Figure 17: Effect of cutter wear state using the models with cutting speed dependency on (a) normal bond strength and (b) grain elastoplasticity.

the cutter upwards under constant force control to regain the force equilibrium. Then the cutting depth is reduced, resulting in a smaller tangential force reaction. Therefore, the reduction in bit torque with increasing rotary speed can be facilitated by the combined axial rate-hardening effects on every single cutter.

4.3. Parameter Sensitivities. The full-scale test drilling [33] has exhibited that the falling torque characteristic is sensitive to WOB and the bit wear state (sharp or dull). To check the reproducibility of these parameter sensitivities in DEM simulations, the influences of typical operating and cutter geometrical parameters on the falling characteristic are further investigated using the cutting scenario with the axial force control. For the operating parameter, the target axial force that corresponds to WOB is varied. In parallel, two different cutter meshes, an unchamfered sharp cutter and a dull cutter, are adopted for investigating the sensitivity to the cutter wear state. Their influences on the falling characteristics are evaluated by the cutter's aggressiveness. The resultant falling characteristics using both rate-dependent models with various axial forces and cutter states are shown in Figures 16 and 17, respectively. It can be seen from Figure 16 that the simulated falling characteristic over RPM becomes more pronounced with a larger target value of the axial force because the axial rate hardening effect is intensified at a larger axial force. The intensification of the rate effect also occurs in Figure 17 with a dull cutter due to the enlarged contact area in the axial direction compared to that of a sharp cutter, resulting in a more significant velocity-weakening characteristic on a dull cutter. These simulated trends are phenomenologically in good agreement with experimental measurements on full bits [33] and thereby confirm the validity of the two proposed modifications. The simulation results also implicate a fundamental possibility to reduce the undesired rate dependency and consequently self-excited drill string vibrations by changing operating conditions or keeping the cutter's sharpness.

5. Conclusion

In this paper, the velocity-dependent cutting process with a PDC cutter is modeled and investigated using the discrete element method. The rock material is modeled by an aggregation of bonded particles, and the rock-cutter interaction in deep drilling environments is investigated through cutting simulations under algorithmically realized hydrostatic confinement.

According to measurements in the pressurized single cutter tests, the axial cutting force is found to have a nonnegligible hardening effect with increasing cutting speed. This phenomenon occurring on the cutter scale is supposed to be responsible for the generally observed unfavorable falling torque characteristic in the drilling process with a PDC drill bit.

To enhance the understanding of this rate dependency, the particle model developed in our previous studies is further modified. Potential modification strategies considering different model complexity and rate indicators on different scales are compared and discussed. Two specific modifications associated with the macroscopic cutting speed are implemented and verified to reproduce the experimentally observed rate dependency: one modifies the normal bond strength in the existing bonded-particle model; the other extends the contact model with an abstract formulation of grain elastoplasticity and then adds the cutting speed dependency to the yield threshold. Both modified models result in a dominant rate hardening effect of the axial cutting force in cutting simulations at a prescribed depth of cut and various cutting speeds.

In addition to qualitatively reproducing the observed rate dependency, further analysis and interpretation of the

simulation results reveal the relationship between the rate-sensitive cutting forces and the causal rock failure mechanisms. The cutting simulation is also extended by implementing a constant axial force control. The averaged tangential force at a steady state is found to decrease with increasing cutting speed, which is consistent with the general falling torque characteristic over RPM on a full bit. Moreover, the influences of axial force and cutter wear state on the falling characteristic are simulatively investigated in this cutting scenario. The corresponding parameter studies indicate that the falling characteristic over RPM intensifies at a higher axial force or with a dull cutter, which is in good qualitative accordance with laboratory full-scale bit tests in the literature. Then the influences of studied parameters on the stability of the drill string system can be evaluated because a more pronounced falling torque characteristic leads to more instable behavior of the drill string and faster self-excitation of torsional vibrations.

This study provides an in-depth discussion on effectively modeling the velocity-dependent cutting process with PDC cutters using the discrete element method. The corresponding simulation results reveal the underlying mechanisms on the single cutter scale that can give a consistent explanation for the experimental observations about the rate sensitivity of the cutting forces on a single cutter and the falling torque characteristic on a full bit. The parameter studies enlighten the possibility of mitigating self-excited drill string vibrations by changing operating states or cutter design. The findings could contribute to a better cutter design that generates less torsional vibrations and a more stable drilling state, thus allowing drilling to achieve a higher rate of penetration.

Future work will focus on investigating the influences of more complex cutter designs (e.g. shaped cutters) on the rate dependency. The rate-dependent cutting simulations will also be coupled with drill string models to study the effect of cutter-rock interaction on drill string dynamics.

Data Availability

The data used to support the findings of this study are included within the article.

Conflicts of Interest

The authors declare that there are no conflicts of interest regarding the publication of this paper.

Acknowledgments

This study was done as part of the employment at the Institute of Dynamics and Vibrations, TU Braunschweig. The corresponding research projects were in collaboration with Baker Hughes. The article processing charge is financially supported by the Open Access Publication Funds of TU Braunschweig.

References

[1] A. Hohl, M. Tergeist, H. Oueslati et al., "Derivation and experimental validation of an analytical criterion for the identification of self-excited modes in drilling systems," *Journal of Sound and Vibration*, vol. 342, pp. 290–302, 2015.

[2] Z. Zhang, Y. Shen, W. Chen, J. Shi, W. Bonstaff, and K. Tang, "Continuous high frequency measurement improves understanding of high frequency torsional Oscillation in North America Land drilling," in *Proceedings of the Day 2 Tue, October 10, 2017. SPE Annual Technical Conference and Exhibition*, San Antonio, Texas, USA, November 2017.

[3] A. Kueck, A. Hohl, C. Schepelmann, S.-L. Lam, D. Heinisch, and C. Herbig, "Break-through in elimination of high-frequency torsional Oscillations through New damping tool proven by field testing in the US," in *Proceedings of the Day 3 Wed, May 04, 2022. Offshore Technology Conference*, Houston, Texas, USA, May 2022.

[4] T. Richard, C. Germay, and E. Detournay, "A simplified model to explore the root cause of stick–slip vibrations in drilling systems with drag bits," *Journal of Sound and Vibration*, vol. 305, no. 3, pp. 432–456, 2007.

[5] J. R. Jain, H. Oueslati, A. Hohl et al., "High-frequency torsional dynamics of drilling systems: an analysis of the bit-system interaction," in *Proceedings of the All Days. IADC/SPE Drilling Conference and Exhibition*, Fort Worth, Texas, USA, July 2014.

[6] G. Pelfrene, H. Sellami, and L. Gerbaud, "Mitigating stick-slip in deep drilling based on Optimization of PDC bit design," in *Proceedings of the SPE/IADC Drilling Conference and Exhibition 2011*, Amsterdam, The Netherlands, March 2011.

[7] M. Amri, G. Pelfrene, L. Gerbaud, H. Sellami, and M. Tijani, "Experimental investigations of rate effects on drilling forces under bottomhole pressure," *Journal of Petroleum Science and Engineering*, vol. 147, pp. 585–592, 2016.

[8] R. R. Hartley and R. P. Behringer, "Logarithmic rate dependence of force networks in sheared granular materials," *Nature*, vol. 421, no. 6926, pp. 928–931, 2003.

[9] O. Matthews, X. Huang, and J. A. Bomidi, "3D simulation Workflow for performance of sharp and Worn PDC drill bits," in *Proceedings of the SPE/IADC International Drilling Conference and Exhibition*, Stavanger in Norway, March 2021.

[10] J. J. Kolle, "A model of dynamic confinement during drilling in pressurized boreholes," *International Journal of Rock Mechanics and Mining Sciences & Geomechanics Abstracts*, vol. 30, no. 7, 1993.

[11] E. Detournay and C. Atkinson, "Influence of pore pressure on the drilling response in low-permeability shear-dilatant rocks," *International Journal of Rock Mechanics and Mining Sciences*, vol. 37, no. 7, pp. 1091–1101, 2000.

[12] M. Amri, G. Pelfrene, E. Jahangir, M. Tijani, and H. Sellami, "Numerical and analytical study of rate effects on drilling forces under bottomhole pressure," *International Journal of Rock Mechanics and Mining Sciences*, vol. 110, pp. 189–198, 2018.

[13] P. Chen, M. Meng, R. Ren et al., "Modeling of PDC single cutter – poroelastic effects in rock cutting process," *Journal of Petroleum Science and Engineering*, vol. 183, Article ID 106389, 2019.

[14] L. W. Ledgerwood, "PFC modeling of rock cutting under high pressure conditions," in *Proceedings of the1st Canada-US Rock Mechanics Symposium*, American Rock Mechanics Association, Vancouver, Canada, May 2007.

[15] H. Huang, B. Lecampion, and E. Detournay, "Discrete element modeling of tool-rock interaction I. Rock cutting," *Int. J. Numer. Anal. Meth. Geomech*, vol. 37, no. 13, pp. 1913–1929, 2013.

[16] C. M. Carrapatoso, G. L. Righetto, C. E. R. Lautenschläger et al., "Numerical modeling of single cutter tests in Carbonates," in *Proceedings of the 49th US Rock Mechanics/ Geomechanics Symposium. OnePetro*, San Francisco, California, June 2015.

[17] W. Liu, X. Zhu, and J. Jing, "The analysis of ductile-brittle failure mode transition in rock cutting," *Journal of Petroleum Science and Engineering*, vol. 163, pp. 311–319, 2018.

[18] R. L. J. Helmons, S. A. Miedema, M. Alvarez Grima, and C. van Rhee, "Modeling fluid pressure effects when cutting saturated rock," *Engineering Geology*, vol. 211, pp. 50–60, 2016.

[19] Q. B. Zhang and J. Zhao, "A Review of dynamic experimental techniques and mechanical Behaviour of rock materials," *Rock Mechanics and Rock Engineering*, vol. 47, no. 4, pp. 1411–1478, 2014.

[20] M. Tergeist, *Partikelmethoden zur Modellierung der Kontakte von Bohrstrang und Gestein beim Tiefbohren*, Dissertation. Institut für Dynamik und Schwingungen, TU Braunschweig, 2019.

[21] Z. Fu, M. Tergeist, A. Kueck, and G.-P. Ostermeyer, "Investigation of the cutting force response to a PDC cutter in rock using the discrete element method," *Journal of Petroleum Science and Engineering*, vol. 213, Article ID 110330, 2022.

[22] S. C. Russell, S. Duffy, and O. Matthews, "Shaped cutter performance Optimization through Advanced drilling simulations," in *Proceedings of the IADC/SPE International Drilling Conference and Exhibition*, Galveston, Texas, USA, March 2022.

[23] H. Oueslati, "Investigations of the PDC Cutter-Rock Interaction as the Root Cause of Torsional Vibrations in Drillstrings," *Diploma Thesis. Leibniz Universität Hannover, Hannover*, vol. 23, 2011.

[24] S. Doshvarpassand, T. Richard, and M. Mostofi, "Effect of groove geometry and cutting edge in rock cutting," *Journal of Petroleum Science and Engineering*, vol. 151, pp. 1–12, 2017.

[25] E. Detournay and P. Defourny, "A phenomenological model for the drilling action of drag bits," *International Journal of Rock Mechanics and Mining Sciences & Geomechanics Abstracts*, vol. 29, no. 1, pp. 13–23, 1992.

[26] D. O. Potyondy and P. A. Cundall, "A bonded-particle model for rock," *International Journal of Rock Mechanics and Mining Sciences*, vol. 41, no. 8, pp. 1329–1364, 2004.

[27] M. Tergeist, H. Oueslati, A. Hohl, and G.-P. Ostermeyer, "Modeling rock cutting under extreme downhole conditions," *Oil Gas: European Magazine*, vol. 42, pp. 29-30, 2016.

[28] N. Rafatian, S. Miska, L. W. W. Ledgerwood, R. Ahmed, M. Yu, and N. Takach, "Experimental study of MSE of a single PDC cutter interacting with rock under simulated pressurized conditions," *SPE Drilling and Completion*, vol. 25, no. 01, pp. 10–18, 2010.

[29] T. Richard, E. Detournay, A. Drescher, P. Nicodeme, and D. Fourmaintraux, "The Scratch test as A Means to measure strength of Sedimentary rocks," in *All Days. SPE/ISRM Rock Mechanics in Petroleum Engineering*, vol. 08, SPE, Trondheim, Norway, 1998.

[30] Z. Cheng, M. Sheng, G. Li et al., "Imaging the formation process of cuttings: characteristics of cuttings and mechanical specific energy in single PDC cutter tests," *Journal of Petroleum Science and Engineering*, vol. 171, pp. 854–862, 2018.

[31] J. A. Mendoza, I. K. Gamwo, W. Zhang, and J. S. Lin, "Discrete element modeling of rock cutting using crushable particles," in *Proceedings of the 44th U.S. Rock Mechanics Symposium and 5th U.S.-Canada Rock Mechanics Symposium: OnePetro*, Salt Lake City, Utah, June 2010.

[32] R. K. Annabattula, Y. Gan, S. Zhao, and M. Kamlah, "Mechanics of a crushable pebble assembly using discrete element method," *Journal of Nuclear Materials*, vol. 430, no. 1-3, pp. 90–95, 2012.

[33] J. F. Brett, "The genesis of torsional drillstring vibrations," *SPE Drill. Eng*, pp. 168–174, 1992.

[34] R. I. Leine, D. H. van Campen, and W. J. G. Keultjes, "Stick-slip whirl interaction in drillstring dynamics," *Journal of Vibration and Acoustics*, vol. 124, no. 2, pp. 209–220, 2002.